

# First-principles prediction of altermagnetism in transition metal graphite intercalation compounds

Weida Fu,<sup>a‡</sup> Guo-Dong Zhao,<sup>b‡</sup> Tao Hu,<sup>a\*</sup> Wencai Yi,<sup>d</sup> Hui Zhang,<sup>b</sup> Alessandro Stroppa,<sup>c</sup> Wei Ren<sup>b</sup> and Zhongming Ren<sup>a</sup>

<sup>a</sup>School of Materials Science and Engineering, State Key laboratory of Advanced Special Steel, Shanghai University, Shanghai, 200241, China

<sup>b</sup>Department of Physics, Materials Genome Institute, International Centre for Quantum and Molecular Structures, Shanghai University, Shanghai 200444, China

<sup>c</sup>CNR-SPIN c/o Università degli Studi dell'Aquila, Via Vetoio 10, I-67010 Coppito (L'Aquila), Italy

<sup>d</sup>Laboratory of High Pressure Physics and Material Science, School of Physics and Physical Engineering, Qufu Normal University, Qufu 273165, China

## ABSTRACT

We report the emergence of altermagnetism, a magnetic phase characterized by the coexistence of compensated spin ordering and momentum-dependent spin splitting, in graphite intercalation compounds (GICs), a prototypical material system long investigated for its tunable electronic and structural properties. Through first-principles calculations, we demonstrate that vanadium-intercalated stage-1 graphite compounds, exhibit inherent altermagnetic properties. The hexagonal crystal system and antiferromagnetic ordering of V atoms generate a magnetic space group ( $P6_3/m'c$ ) that enforces alternating spin polarization in momentum space while maintaining zero net magnetization. The calculated band structure reveals robust altermagnetic signatures: along the  $M_2' - \Gamma - M_2$  high-symmetry direction, we observe a pronounced spin splitting of  $\sim 270$  meV with alternating spin polarization. Crucially, the spin splitting exhibits minimal sensitivity to spin-orbit coupling (SOC) effect, highlighting the dominance of exchange interactions over relativistic effects. From Monte Carlo simulations, we predict a magnetic transition temperature ( $T_m$ ) of  $\sim 228$  K, indicating stable magnetic ordering above liquid nitrogen temperatures. The combination of symmetry-protected spin textures, SOC-independent splitting, and elevated  $T_m$  temperature makes V-GICs as a promising candidate for spintronic applications, particularly for zero-field spin-polarized current generation and topologically robust spin transport. As the first demonstration of carbon-based alternating magnetic systems, this work offers a design paradigm for engineering spin-polarized quantum states governed by crystalline symmetry constraints.

**KEYWORDS:** Altermagnetism, transition metal, graphite intercalation compounds, first principles.

## INTRODUCTION

The recent discovery of altermagnetism [1-5], a collinear magnetic phase characterized by non-trivial spin group symmetry, has expanded the conceptual framework of quantum magnetism while offering considerable potential for spintronic applications [6-9]. This emergent phase combines three defining characteristics: robust time-reversal symmetry breaking enabling spin-polarized electronic states, antiparallel magnetic ordering maintaining zero net magnetization, and momentum-dependent alternating spin-split band structures [10-14]. Unlike conventional ferromagnetism or antiferromagnetism, altermagnetism arises from specific crystallographic constraints, being strictly confined to 37 spin point groups where sublattice symmetry operations form index-2 subgroups of the parent crystal structure [15-20]. Such symmetry-engineered hybridization creates

unique quantum phenomena previously considered mutually exclusive in traditional magnetic classifications, as evidenced by experimental confirmations of theoretically predicted signatures including anomalous Hall/Nernst effects, nonlinear spin currents, and magneto-optical responses [21-23]. While these breakthroughs validate the unique symmetry-broken states and device potential of altermagnetism, which has been identified in numerous metallic compounds [24,25], no verified altermagnetic phases have been reported in carbon-based materials. This challenge motivates re-examination of established material platforms through the lens of symmetry-controlled magnetism.

Graphite intercalation compounds (GICs) is a traditional material system that has been extensively studied, with leading researchers Dresselhaus uncovering a vast range of fascinating properties [26,27]. From a symmetry perspective, intercalated

graphite has great potential as a platform for discovering and harnessing unique magnetic phenomena like altermagnetism. The layered structure of graphite allows for the controlled insertion of transition metals [28], which can introduce local magnetic moments and disrupt the symmetry of the system. This symmetry breaking, coupled with the interaction between the intercalant's d-electrons and the  $\pi$ -electrons of graphite [29], can give rise to complex magnetic orders, including altermagnetism. Therefore, the tunable electronic and magnetic properties of intercalated graphite make it a promising candidate for studying the emergence of altermagnetism and its associated phenomena.

In this work, we systematically investigate the emergence of altermagnetism in transition metal-intercalated graphite from a symmetry perspective, employing first-principles calculations to validate this novel magnetic phase. Our calculations identify vanadium graphite intercalation compounds (V-GICs) as a robust altermagnetic host, exhibiting momentum-dependent spin-split band structures along specific high-symmetry paths. Crucially, these spin-split bands demonstrate minimal sensitivity to spin-orbit coupling (SOC) effects, with splitting energies governed primarily by exchange interactions. The system exhibits a magnetic anisotropy energy (MAE) of 0.6 meV per formula unit and stabilizes out-of-plane magnetic moments, as revealed by relativistic calculations. Monte Carlo simulations further predict a magnetic transition temperature ( $T_m$ ) of  $\sim 228$  K, demonstrating robust magnetic ordering stability within the operational temperature range for practical applications. This study not only unravels the fundamental mechanisms driving altermagnetism in layered intercalation compounds but also establishes a design paradigm for engineering quantum materials with programmable magnetic and electronic functionalities. The subsequent sections detail our computational methodology, present comprehensive results across atomic structure, electronic properties, and magnetic, and provide comparative analyses with conventional magnetic systems.

## METHODS

The density functional theory (DFT) calculations described in this paper were implemented in the Vienna ab initio simulation package (VASP) code [30-32]. The atomic-scale simulation models were developed using Device Studio, a comprehensive computational package created by Hongzhiwei Technology (Shanghai) Co., Ltd., which specializes in crystal structure design, molecular visualization, and scientific data processing. DFT computations were partially conducted through the integrated Projector-

Augmented Wave (PAW) method implementation within the DS-PAW software suite. PAW potentials were employed to describe the interaction between valence electrons and ion core [33,34], ensuring accurate representation of the electronic structure. A plane-wave basis set with a kinetic energy cutoff of 500 eV was utilized, and the Brillouin zone was sampled using a  $9 \times 9 \times 4$   $\Gamma$ -centered Monkhorst-Pack  $k$ -grid for both relaxation and electronic structure calculations. To account for the correlation energy of the strongly localized 3d orbitals of transition metals (TM), the Hubbard U correction (DFT+U) was applied [35,36], with the Dudarev type [37,38], utilizing the exchange-correlation functional of Perdew-Burke-Ernzerhof (PBE) [39] type in generalized gradient approximation (GGA). Previous studies of TM-adsorbed graphene systems using GGA+U have shown consistency with results obtained from the B3LYP hybrid functional, providing a robust validation of this approach [40]. All structures were fully relaxed without imposing symmetry constraints, with convergence criteria of  $10^{-7}$  eV per cell for energy and 0.001 eV/Å for atomic forces. The intercalation energy ( $E_{ic}$ ) was defined as  $E_{ic} = E_{VIC} - E_V - E_g$ ,  $E_{VIC}$ ,  $E_V$  and  $E_g$  are the energies of the intercalated compounds states of  $C_{16}V_2$ , V atoms and bulk graphite. It is essentially the formation energy of the compound and is used to assess the thermodynamic stability of the system [41,42]. To investigate the dynamic and thermal stabilities, phonon spectra are simulated with the density functional perturbation theory (DFPT) by the Phonopy code, and the Ab initio Molecular Dynamics (AIMD), the cutoff energy of 400 eV was set and the energy convergence criterion was set to  $2 \times 10^{-5}$  eV. As supercell contains nearly 486 atoms, only the  $\Gamma$ -point sampling was used to sample the Brillouin zone. Molecular dynamics simulations were carried out using the canonical (NVT) ensemble at a temperature of 300 K for a duration of 10 ps with a time step of 2 fs. The Nose-Hoover thermostat was utilized to maintain the system temperature, as its stochastic nature is well-suited for phase space sampling. The spin-orbit coupling (SOC) is considered for different spin orientations in the magnetic anisotropy energy (MAE) calculations with the energy convergence criteria of  $10^{-8}$  eV as  $MAE = E[100] - E[001]$ . Classical Metropolis Monte Carlo (MC) simulations of the Heisenberg model [43,44] were performed to calculate the magnetic phase transition temperatures with  $10 \times 10$  supercell, 4000 temperature points. On each temperature point,  $10^5$  Monte Carlo steps were performed for equilibrium and another  $10^5$  steps were performed for statistics [45]. The specific heat  $C_v = \frac{\langle E^2 \rangle - \langle E \rangle^2}{Nk_B T^2}$  where E is the total energy, N is the number of magnetic ions,  $k_B$  is the Boltzmann

\*Contact author: taohu@shu.edu.cn

‡ Labelled as co-first author of the paper

constant, and  $T$  is the temperature. The corresponding methods of magnetic constants extraction are provided in the main text.

## RESULTS and DISCUSSION

The core challenge in achieving altermagnetism lies in the precise design of symmetry breaking, particularly at the crystal structure level. This challenge can be summarized as follows. First, the establishment of a magnetic ordered state necessitates the breaking of time-reversal symmetry (T), which is a prerequisite for the generation of spin-polarized electronic bands. While breaking time-reversal symmetry, it is crucial to maintain the joint operation formed by both the magnetic order and crystal symmetry, such as  $T \cdot C_n$  (time-reversal coupled with  $n$ -fold rotation) or  $T \cdot M$  (time-reversal combined with

mirror reflection), which ensures the alternating distribution of spin polarization in momentum space, ultimately achieving zero net magnetization.

The classic system of intercalated graphite precisely meets these requirements. The specific system investigated in this study,  $C_{16}X_2$ , featuring transition metal intercalation in graphite, exhibits key structural characteristics: it adopts a hexagonal crystal system with space group  $P6_3mc$  (No.186), 6mm point group. Through first-principles calculations of the magnetic ground state of various transition metal intercalated graphite, we found that transition metal intercalated graphite compounds (GICs) perfectly satisfies the above conditions. The detailed calculation results are presented in Table 1. Furthermore, by utilizing the AMCHECK package [46], we confirmed that the system fulfills the criteria for altermagnetic ordering when its net magnetic moment vanishes.

TABLE I. Magnetic Ground States of Transition Metal-Intercalated Graphite Compounds. AFM and FM denote antiferromagnetic and ferromagnetic ordering ground states, respectively, in transition metal-intercalated graphite compounds.  $\Delta E$  denotes the energy difference between AFM and FM states per formula units. The magnetic moments listed are those of the transition metal atoms.

TM	V	Cr	Mn	Fe	Co
Magnetic Ground State	AFM	FM	FM	FM	FM
$\Delta E$ (eV)	0.251	0.401	0.703	0.153	0.125
$U_{\text{eff}}$ (eV)	5.0	3.4	4.8	5.1	6.2
Magnetic Moment ( $\mu B$ )	2.63	3.51	3.10	2.17	1.77

We characterized the crystal structure of vanadium graphite intercalation compounds (V-GICs) revealing a stage-1 configuration with unit cell composition  $C_{16}V_2$ . The compound crystallizes in a hexagonal system (space group  $P6_3m'c$ , No.186.205) with lattice parameters  $a = b = 5.011 \text{ \AA}$  and  $c = 7.286 \text{ \AA}$ , and unit cell angles  $\alpha = \beta = 90^\circ$  and  $\gamma = 120^\circ$ , consistent with layered intercalation symmetry. The symmetry operations combine a magnetic mirror plane  $m'$  with  $6_3$  screw axes along  $[001]$ , forming a polar structure lacking inversion symmetry. Vanadium atoms occupy the 2b Wyckoff positions (multiplicity 2) between carbon layers, where equivalent positions are generated through  $6_3$  screw operations coupled with time-reversal symmetry T, enforcing antiparallel spin alignment along  $c$ -axis. Carbon sublattices maintain hexagonal symmetry through 6c Wyckoff sites (multiplicity 6) with zero net magnetization, as shown in Figure 1(a, b). This magnetic configuration preserves the parent graphite's hexagonal framework while introducing ordered V intercalates, where the altermagnetic order emerges from the interplay

between  $6_3$  screw-axis mediated structural symmetry and antiferromagnetic exchange coupling along the  $c$ -axis.

To investigate the structural stability of V-GICs, we performed AIMD simulations on the supercell structure at room temperature. Under thermal perturbations, all atoms exhibited regular thermal vibrations while maintaining structural integrity without significant distortion, with the final configuration visualized in Figure 1(c). The time evolution profiles of total energy, temperature, and atomic forces (Fig. 1d) demonstrate excellent convergence throughout the simulation. The temperature oscillates within  $300 \pm 30 \text{ K}$  while the total energy variation remains below  $0.001 \text{ eV/atom}$ . These computational results collectively confirm that the system exhibits excellent structural stability under ambient conditions. The intercalated energy ( $E_{ic}$ ) is  $-0.93 \text{ eV}$  per V atom, where a negative value indicates an exothermic intercalated, indicating that the V-GICs is thermodynamically stable.

\*Contact author: taohu@shu.edu.cn

† Labelled as co-first author of the paper

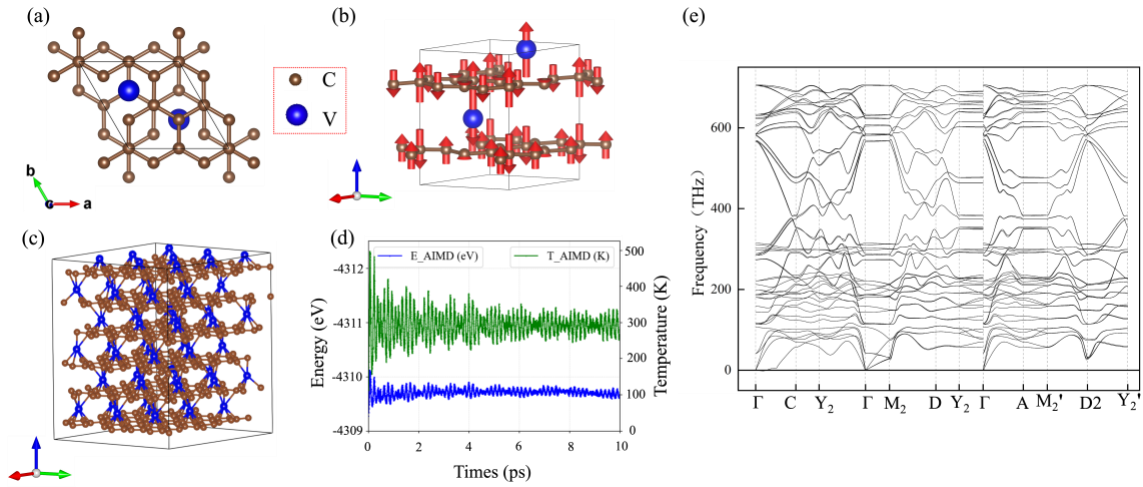


FIG 1. (a) the top view and (b) the Cross-sectional view of the V-GICs structure. Red arrows indicate the magnitude and orientation of the magnetic moments, the vanadium atomic magnetic moments are depicted at their actual scale, whereas those of carbon atoms are artificially enhanced twentyfold for enhanced visual clarity. (c) Cross-sectional view of the  $3 \times 3 \times 3$  supercell structure for vanadium-intercalated graphite after 10 ps AIMD simulation at ambient conditions, demonstrating structural relaxation to thermodynamic equilibrium. (d) Time evolution profiles of temperature fluctuation (green curve) and energy convergence (blue curve) during MD simulation. (e) Phonon band structures representing dynamic stabilities.

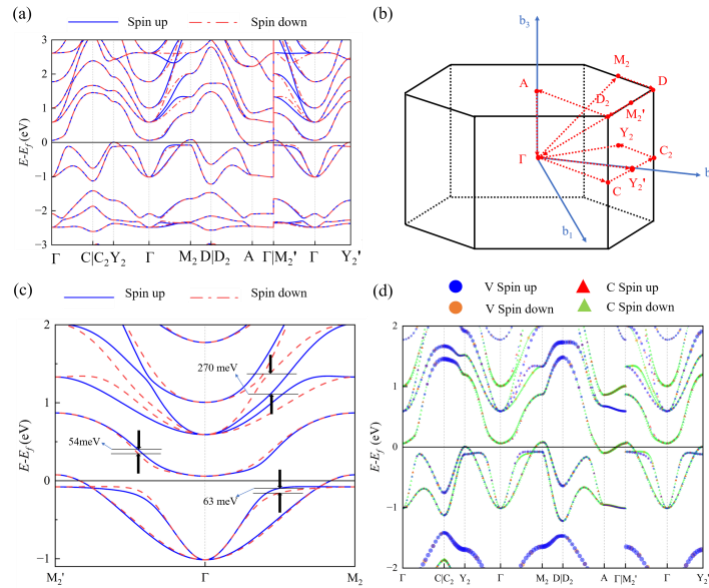


FIG 2. (a) Calculated spin-polarized band structure of the V-GICs, illustrating the energy dispersion of spin-up and spin-down states across the Brillouin zone. (b) The first Brillouin zone of the V-GICs, along with the high-symmetry points path used in the band structure calculations. Panel (c) highlighting the splitting along the  $M_2'-\Gamma-M_2$  direction, the calculated band dispersion exhibits alternating spin polarization across the gamma point, some of the band splitting values are also labelled. (d) The fat energy band diagram of the density of states contributions, where the different color shapes of the bubbles represent the contributions of the different elements and spins, respectively. The size of the bubble indicates the weight of its contribution.

The electronic band structure of the V-GICs system provides a crucial perspective for understanding its alternating magnetic properties. As

shown in Figure 2(a) and 2(c), the spin-resolved band structure reveals the unique spin polarization behavior of the system with zero net magnetization. The spin-

\*Contact author: taohu@shu.edu.cn

† Labelled as co-first author of the paper

up and spin-down bands exhibit significant momentum-dependent characteristics along high-symmetry paths in the Brillouin zone. Specifically, along the  $M_2'$ - $\Gamma$ - $M_2$  direction, the maximum spin-splitting energy gap reaches approximately 270 meV, while along the  $Y_2'$ - $\Gamma$ - $Y_2$  direction, the bands remain degenerate. Near the Fermi energy level, its conduction and valence bands exhibit band splitting at 54 and 63 meV, respectively. This coexistence of alternating spin polarization and degeneracy directly reflects the spin-momentum locking mechanism protected by symmetry in the alternating magnetic properties. The orbital-projected band structure of V-GICs reveals the electronic contributions from vanadium and carbon atoms in both spin channels. These two elements exhibit indistinguishable contributions across the energy spectrum, demonstrating strong hybridization effects between their atomic orbitals. This complete merging of electronic states suggests the formation of coherent hybridized bands with significant covalent bonding characteristics.

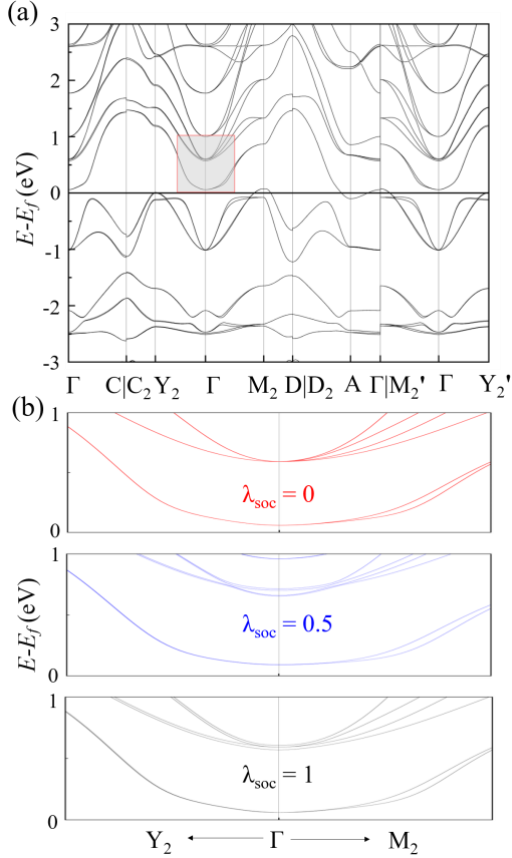


FIG 3. The band structure considering spin-orbit coupling, highlighting the splitting along the  $\Gamma$ - $M_2$  direction and the degeneracy along the  $\Gamma$ - $Y_2$  direction.

The alternating magnetic band splitting in V-GICs reveals a fundamentally different physical origin compared to traditional magnetic systems. The splitting of its spin-polarized bands is primarily driven by exchange interactions and the breaking of crystal symmetry, rather than relying on spin-orbit coupling (SOC) effects. To investigate the effect of SOC strength on band structures, we introduce a scaling factor  $\lambda_{\text{SOC}}$  to the SOC Hamiltonian term within the DFT framework [47]. The SOC Hamiltonian is expressed as:

$$\mathcal{H}_{\text{SOC}} = \lambda_{\text{SOC}} \left( \frac{\hbar^2}{2m_e^2 c^2} \frac{K(r)}{r} \frac{dV(r)}{dr} \hat{L} \cdot \hat{S} \right) \quad (1)$$

where  $\hat{L} = \hat{r} \times \hat{P}$  is the orbital angular momentum operator,  $\hat{S}$  is the spin operator,  $V(r)$  is the spherical part of the effective all-electron potential within the PAW sphere, and  $K(r) = \left(1 - \frac{V(r)}{2m_e c^2}\right)^{-2}$ . All Hamiltonians, wave functions, charge densities, and potentials are calculated self-consistently. Figure 3(a) presents the band structure with SOC effects included, revealing a small band splitting at the  $\Gamma$  point compared to the SOC = 0 case. However, this SOC-induced splitting has negligible impact on the overall band structure, particularly the existing spin-split bands. This observation is further corroborated by the magnified band structures in Figure 3(b), which compare the cases of  $\lambda_{\text{SOC}} = 0, 0.5,$  and  $1$ . The results consistently demonstrate that the primary band splitting remains largely unaffected by SOC strength, indicating that the spin-polarized band structure is predominantly governed by exchange interactions and symmetry-breaking mechanisms rather than SOC effects. This unique feature distinguishes the system from conventional topological materials, which typically require strong SOC or external fields to induce band splitting. The weak dependence on SOC suggests that the system can achieve significantly longer spin relaxation times ( $\tau_s$ ) due to reduced spin-flip scattering, as  $\tau_s$  is inversely proportional to the square of SOC strength. Additionally, the SOC-independent band splitting enhances temperature stability, as the spin-polarized states are less susceptible to thermal fluctuations that typically degrade SOC-driven effects. These advantages make the system a promising candidate for high-performance spintronic devices operating at finite temperature.

\*Contact author: taohu@shu.edu.cn

† Labelled as co-first author of the paper

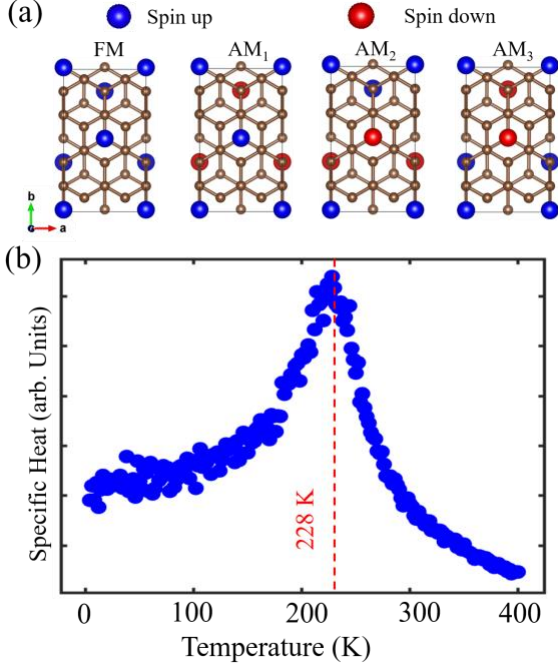


FIG 4. (a) Schematic representation of the magnetic exchange interaction of V-GICs supercells with hexagonal structure. Including nearest and next-nearest neighbor spin exchanges. The brown spheres represent carbon atoms, and the red and blue spheres represent vanadium atoms with spin up and spin down, respectively. (b) Specific heat versus temperature from Monte Carlo simulations, transition temperature is estimated as  $\sim 228$  K.

First-principles calculations incorporating SOC reveal a moderate magnetic anisotropy energy (MAE) of 0.6 meV per formula unit, with the easy axis aligned along the crystallographic [001] direction (Fig. 1b). This MAE magnitude, comparable to benchmark 2D  $\text{VI}_3$  (0.8 meV) and  $\text{CrI}_3$  (0.6 meV) [45], suggesting comparable spin-orbital locking strength. To account for the effects of finite anisotropy and avoid overestimating the  $T_m$ , we performed Monte Carlo simulations based on the Heisenberg model. The four supercell configurations (Fig. 4a) exhibit distinct energetic hierarchies: FM,  $\text{AM}_1$  (ground state),  $\text{AM}_2$ , and  $\text{AM}_3$ , with energy differentials relative to  $\text{AM}_1$  measuring 0.11 eV, 0.38 eV, and 0.65 eV, respectively. The system can be effectively simplified to a hexagonal lattice, as illustrated in Figure 4(a), and described by an effective spin Hamiltonian that captures the magnetic interactions within the system.

$$\mathcal{H}_{\text{heisenberg}} = -2J_1 \sum_{\langle i,j \rangle} S_i \cdot S_j - 2J_2 \sum_{\langle\langle i,j \rangle\rangle} S_i \cdot S_j - D \sum_i |S_i^z|^2 \quad (2)$$

\*Contact author: taohu@shu.edu.cn

† Labelled as co-first author of the paper

Here,  $J_1$ ,  $J_2$  and  $J_3$  represent the isotropic exchange parameters for the first, second and third nearest neighbors, respectively, where  $\langle ij \rangle$  and  $\langle\langle ij \rangle\rangle$  denote the corresponding nearest-neighbor and next-nearest-neighbor pairs.  $D$  represents the single-ion anisotropy term, which accounts for the anisotropic magnetic interactions. Since the MAE and isotropic exchange parameters from the graphite is relatively weak, only the MAE and isotropic exchange parameters of V is considered in calculating, and the MAE of C atoms is assumed to be zero. The energy expressions for the four systems illustrated in Figure 4a can be written sequentially as follows:

$$\begin{aligned} E_{\text{FM}} &= -E_0 - (3J_1 + 6J_2 + 3J_3)|\vec{S}|^2 - D|\vec{S}_z|^2 \\ E_{\text{AM}_1} &= -E_0 - (-3J_1 + 6J_2 - 3J_3)|\vec{S}|^2 - D|\vec{S}_z|^2 \\ E_{\text{AM}_2} &= -E_0 - (3J_1 + 6J_2 - 3J_3)|\vec{S}|^2 - D|\vec{S}_z|^2 \\ E_{\text{AM}_3} &= -E_0 - (-3J_1 + 6J_2 + 3J_3)|\vec{S}|^2 - D|\vec{S}_z|^2 \quad (3) \end{aligned}$$

The calculated exchange interaction parameters are determined to be  $J_1 = -2.9265$  meV,  $J_2 = -8.4963$  meV, and  $J_3 = 5.5974$  meV. The specific heat curves in Figure 4 (b) show that the  $T_m$  for V-GICs is  $\sim 228$  K. A series of previous studies have also shown that it is possible to continue to modulate its phase transition temperature by applying strain.

## CONCLUSION

In summary, this work establishes V-GICs ( $\text{C}_{16}\text{V}_2$ ) as a prototypical altermagnet, leveraging symmetry engineering to realize a compensated magnetic phase with momentum-dependent spin polarization. By combining first-principles calculations and symmetry analysis, we demonstrate that the hexagonal crystal structure ( $\text{P6}_3\text{mc}$ ) and antiferromagnetic ordering of vanadium atoms generate a magnetic space group ( $\text{P6}_3\text{m}'\text{c}$ ) that enforces alternating spin-split band structures while preserving zero net magnetization. Key features of the altermagnetic phase—robust spin splitting ( $\sim 270$  meV along  $\text{M}_2'-\Gamma-\text{M}_2$ ) and spin-degeneracy along symmetry-protected directions (e.g.,  $\text{Y}_2'-\Gamma-\text{Y}_2$ ), emerge directly from the interplay between crystallographic symmetry and magnetic order. Crucially, the spin splitting exhibits negligible dependence on spin-orbit coupling (SOC), underscoring the dominance of exchange interactions over relativistic effects and suggesting enhanced spin transport properties with prolonged spin relaxation times. Monte Carlo simulations further predict a magnetic transition temperature ( $T_m$ ) of  $\sim 228$  K, positioning this system among the rare class of altermagnets capable of sustaining magnetic order above liquid nitrogen temperatures. The synergy between symmetry-protected spin textures, SOC-independent splitting, and elevated  $T_m$  highlights the

unique advantages of V-GICs for practical spintronic applications, including zero-field spin-polarized current generation and topologically robust spin manipulation. These findings not only advance intercalated graphite as a tunable platform for exploring altermagnetism but also provide a blueprint for designing symmetry-driven quantum materials. Future efforts could extend this approach to other transition metal-graphite systems, optimize interfacial coupling in heterostructures, and explore crossover phenomena between altermagnetism and topological states.

## ACKNOWLEDGMENTS

This work was supported by the National Key Research and Development Program of China (Grants No. 2024YFB3713803), the Key Program of the National Natural Science Foundation of China (Grants No. 52274386). This work was also supported by Shanghai Technical Service Center of Science and Engineering Computing, Shanghai University.

## Reference

- [1] L. Bai, W. Feng, S. Liu, L. Šmejkal, Y. Mokrousov, and Y. Yao, *Adv. Funct. Mater.* **34** (49) (2024), 2409327 doi:10.1002/adfm.202409327
- [2] P. Das, V. Leeb, J. Knolle, and M. Knap, *Phys Rev Lett* **132** (26) (2024), 263402 doi:10.1103/PhysRevLett.132.263402
- [3] S. W. Lovesey, D. D. Khalyavin, and G. van der Laan, *Phys. Rev. B* **108** (12) (2023), 121103 doi:10.1103/PhysRevB.108.L121103
- [4] I. Mazin, *Physics* **17** (4) (2024) doi:10.1103/Physics.17.4
- [5] L. Šmejkal, J. Sinova, and T. Jungwirth, *Phys. Rev. X* **12** (4) (2022), 040501 doi:10.1103/PhysRevX.12.040501
- [6] J. Ding *et al.*, *Phys Rev Lett* **133** (20) (2024), 206401 doi:10.1103/PhysRevLett.133.206401
- [7] S. Giuli, C. Mejuto-Zaera, and M. Capone, *Phys. Rev. B* **111** (2) (2025), 020401 doi:10.1103/PhysRevB.111.L020401
- [8] H.-Y. Ma and J.-F. Jia, *Phys. Rev. B* **110** (6) (2024), 064426 doi:10.1103/PhysRevB.110.064426
- [9] R. W. Zhang, C. Cui, R. Li, J. Duan, L. Li, Z. M. Yu, and Y. Yao, *Phys Rev Lett* **133** (5) (2024), 056401 doi:10.1103/PhysRevLett.133.056401
- [10] Z. Liu, M. Ozeki, S. Asai, S. Itoh, and T. Masuda, *Phys Rev Lett* **133** (15) (2024), 156702 doi:10.1103/PhysRevLett.133.156702
- [11] P. A. McClarty and J. G. Rau, *Phys Rev Lett* **132** (17) (2024), 176702 doi:10.1103/PhysRevLett.132.176702
- [12] S. Sheoran and S. Bhattacharya, *Phys. Rev. Mater.* **8** (5) (2024), 051401 doi:10.1103/PhysRevMaterials.8.L051401
- [13] L.-D. Yuan, Z. Wang, J.-W. Luo, E. I. Rashba, and A. Zunger, *Phys. Rev. B* **102** (1) (2020), 014422 doi:10.1103/PhysRevB.102.014422
- [14] S. Zeng and Y.-J. Zhao, *Phys. Rev. B* **110** (17) (2024), 174410 doi:10.1103/PhysRevB.110.174410
- [15] P. G. Radaelli, *Phys. Rev. B* **110** (21) (2024), 214428 doi:10.1103/PhysRevB.110.214428
- [16] M. Roig, A. Kreisel, Y. Yu, B. M. Andersen, and D. F. Agterberg, *Phys. Rev. B* **110** (14) (2024), 144412 doi:10.1103/PhysRevB.110.144412
- [17] S. Rooj, S. Saxena, and N. Ganguli, *arXiv* **2406** (2024), .06232v1
- [18] L. Šmejkal, J. Sinova, and T. Jungwirth, *Phys. Rev. X* **12** (3) (2022), 031042 doi:10.1103/PhysRevX.12.031042
- [19] I. Turek, *Phys. Rev. B* **106** (9) (2022), 094432 doi:10.1103/PhysRevB.106.094432
- [20] S. Zeng and Y.-J. Zhao, *Phys. Rev. B* **110** (5) (2024), 054406 doi:10.1103/PhysRevB.110.054406
- [21] X. Zhou, W. Feng, R. W. Zhang, L. Smejkal, J. Sinova, Y. Mokrousov, and Y. Yao, *Phys Rev Lett* **132** (5) (2024), 056701 doi:10.1103/PhysRevLett.132.056701
- [22] Y. Zhu, T. Chen, Y. Li, L. Qiao, X. Ma, C. Liu, T. Hu, H. Gao, and W. Ren, *Nano Lett* **24** (1) (2024), 472 doi:10.1021/acs.nanolett.3c04330
- [23] I. Khan, D. Bezzerga, and J. Hong, *Mater Horiz* (2025) doi:10.1039/d4mh01619j
- [24] Y. Che, Y. Chen, X. Liu, H. Lv, X. Wu, and J. Yang, *JACS Au* **5** (1) (2025), 381 doi:10.1021/jacsau.4c01150
- [25] R. Wilkinson, *Physics* **17** (2024) doi:10.1103/Physics.17.s10
- [26] M. S. Dresselhaus and G. Dresselhaus, *Adv Phys* **30** (2) (2006), 139 doi:10.1080/00018738100101367
- [27] T. Enoki, M. Endo, and M. Suzuki, *Graphite Intercalation Compounds and Applications* (Oxford University Press, 2003).
- [28] W. Zhao, P. H. Tan, J. Liu, and A. C. Ferrari, *JACS* **133** (15) (2011), 5941 doi:10.1021/ja110939a
- [29] Y. Li, Y. Lu, P. Adelhelm, M.-M. Titirici, and Y.-S. Hu, *Chem. Soc. Rev.* **48** (17) (2019), 4655 doi:10.1039/c9cs00162j
- [30] G. Kresse and J. Furthmüller, *Comp. Mater. Sci.* (6) (1996), 15
- [31] G. Kresse and J. Furthmüller, *Phys. Rev. B* **54** (16) (1996), 11169 doi:<https://doi.org/10.1103/PhysRevB.54.11169>

\*Contact author: taohu@shu.edu.cn

‡ Labelled as co-first author of the paper

- [32] P. Hohenberg and W. Kohn, *Physical Review* **136** (3B) (1964), B864  
doi:10.1103/PhysRev.136.B864
- [33] P. E. Blochl, *Phys. Rev. B Condens Matter* **50** (24) (1994), 17953 doi:10.1103/physrevb.50.17953
- [34] G. Kresse and D. Joubert, *Phys. Rev. B* **59** (3) (1999), 1758  
doi:<https://doi.org/10.1103/PhysRevB.59.1758>
- [35] S. L. Dudarev, G. A. Botton, S. Y. Savrasov, C. J. Humphreys, and A. P. Sutton, *Phys. Rev. B* **57** (3) (1998), 1505  
doi:<https://doi.org/10.1103/PhysRevB.57.1505>
- [36] V. I. Anisimov, F. Aryasetiawan, and A. I. Lichtenstein, *J. Condens. Matter Phys* **9** (9) (1997), 767 doi:10.1088/0953-8984/9/4/002
- [37] J. He, S. Y. Ma, P. Zhou, C. X. Zhang, C. He, and L. Z. Sun, *J. Phys. Chem. C* **116** (50) (2012), 26313 doi:10.1021/jp307408u
- [38] J. Neugebauer and M. Scheffler, *Phys Rev B Condens Matter* **46** (24) (1992), 16067  
doi:10.1103/physrevb.46.16067
- [39] J. P. Perdew, K. Burke, and M. Ernzerhof, *Phys. Rev. Lett.* **77** (18) (1996), 3865  
doi:<https://doi.org/10.1103/PhysRevLett.78.1396>
- [40] T. O. Wehling, E. Sasioglu, C. Friedrich, A. I. Lichtenstein, M. I. Katsnelson, and S. Blugel, *Phys. Rev. Lett.* **106** (23) (2011), 236805  
doi:10.1103/PhysRevLett.106.236805
- [41] S. B. Mishra, E. T. Marcial, S. Debata, A. N. Kolmogorov, and E. R. Margine, *Phys. Rev. B* **110** (17) (2024), 174508 doi:10.1103/PhysRevB.110.174508
- [42] Y. Zhao, Y. Wang, Y. Yang, J. Zhao, and X. Jiang, *npj Comp. Mater.* **10** (1) (2024), 122  
doi:10.1038/s41524-024-01301-x
- [43] N. Metropolis and S. Ulam, *JASA* **44** (247) (1949), 335 doi:10.1080/01621459.1949.10483310
- [44] G. D. Zhao, W. Fu, Y. Li, X. Liu, F. Jia, T. Hu, and W. Ren, *ACS Appl Mater Interfaces* **16** (1) (2024), 1268 doi:10.1021/acsami.3c09270
- [45] G.-D. Zhao, X. Liu, T. Hu, F. Jia, Y. Cui, W. Wu, Whangbo, Myung-Hwan, and W. Ren, *Phys. Rev. B* **103** (1) (2021), 014438  
doi:10.1103/PhysRevB.103.014438
- [46] A. Smolyanyuk, L. Šmejkal, and I. I. Mazin, *SciPost Physics Codebases* (2024)  
doi:10.21468/SciPostPhysCodeb.30
- [47] S. Steiner, S. Khmelevskiy, M. Marsmann, and G. Kresse, *Phys. Rev. B* **93** (22) (2016), 224425  
doi:10.1103/PhysRevB.93.224425

\*Contact author: taohu@shu.edu.cn

‡ Labelled as co-first author of the paper